

**Synthesis of fluorescent Carbon dots using bio-waste powder for photo-degradation of dyes:
Simulation and Mechanistic Study**

Pranshu Kumar Gupta ^a, Kalluri V. S. Ranganath ^{a*}

^aDepartment of Chemistry, Centre of Advanced Study, Institute of Science, Banaras Hindu University, Varanasi-221005, Uttar Pradesh, India

Electronic Supplementary Information

Contents

S. No.	Particulars	Page No.
S1	Materials and methods	2
S2	Absorption Spectra and Tauc Analysis (Table S1)	3
S3	Fluorescence Maxima Estimation (Figure S1, Table S2)	5
S4	Quantum Yield Estimation (Table S3)	6
S5	Powder X-ray Diffraction (Table S4)	7
S6	XPS Spectroscopy (Figure S2)	8
S7	FTIR Spectroscopy (Figure S3-S5, Table S5)	9
S8	Dynamic Light Scattering Analysis (Figure S6)	12
S9	Brus Kayanuma Calculations	13
S10	VMD Simulation of SCCQDs (Figure S7, Table S6)	13
S11	CHN Analysis of SCCQDs (Table S7)	17
S12	Calculation of E_{VB} and E_{CB} values	18
S13	Sunlight mediated Photodegradation of MB dye (Figure S8-S11)	18
S14	Analysis of SCCQDs-R5 (Figure S12-S13)	22
S15	Mechanistic study of MB dye degradation (Figure S14-S18)	23
S16	Previous reports synthesis and application of Sugarcane bagasse derived CQDs (Table S8)	26

S1. Materials and methods

Tender leaf-bearing branches of sugarcane bagasse were identified and collected as a biowaste from Institute of Agricultural Science, Banaras Hindu University, Varanasi-221005, Uttar Pradesh, India. Hydrothermal treatment of the bagasse powder was done using a rectangular Muffle Furnace (NSW 101 model, Navarang make, MFI: 100 x 100 x 225) in Techinstro M1011 25.0 mL Hydrothermal bomb. Aqueous solutions of SCCQDs and MB-dye degradation kinetics were studied on Shimadzu UV-visible spectrophotometer (Model: UV-1700). The direct allowed e/h transition ($n = 0.5$) band gaps (E_g) were deduced from Tauc plot. The fluorescence measurements were carried out using a Horiba Jobin-Yvon Spectrofluorometer (Model: Fluorolog FL-3-11) and quantum yield calculation was done *w.r.t.* Quinine Sulphate. The hydrodynamic radii, polydispersity index and surface potential of 10 mg/L aqueous CQD solution was estimated through Malvern PAN analytical Zetasizer (Model: ZSU5700; $n = 2.33$; $k = 0.34$). Powder characteristics of materials were analyzed through high resolution Bruker Advance Powder X-ray Diffractometer (Model: D8) using Cu $K_{\alpha 1}$ radiation with Ni filter (40kV x 40 mA). Williamson Hall size analysis, peak indexing and de-phasing (via JCPDS cards) were performed using PAN analytical X'-pert High score Plus Version-3.0, 2009 and Pearson's Crystal Database (2010/11 ASM International Materials Park, Ohio, USA). Binding energies of SCCQDs were estimated using Thermo VG Scientific X-ray Photoelectron Spectrophotometer (XPS; Make: VERSAPROBE; Model: PHI5000) using Al K_{α} radiation (Model: ESCALAB250; 15 kV x 150 V; $SD \sim 500 \mu\text{m}$), with transmission function calibrated using standard Cu sample, after deducting the binding energy offset of 1.9975 ± 0.0825 eV. Bond vibration analysis was done via Fourier-Transform Infrared (FT-IR) spectrophotometer (Make: JASCO; Model: FT/IR-4700; ν : $4000\text{-}500 \text{ cm}^{-1}$), by preparing KBr pellets of respective samples. Size, composition and morphology of SCCQDs were further analyzed by scanning electron microscopy (SEM). Energy dispersive X-ray spectroscopy (EDX) was performed by preparing a thin film of SCCQDs by spin coating (1500 rpm) method, applied on a clean aluminum foil ($1 \text{ cm} \times 1 \text{ cm}$) and dropping approximately $100 \mu\text{l}$ of sample then allowed to dry for 30–40 min, at room temperature, and subjected it to SEM instrument (Model: FEI Quanta 250). Particle size was accurately determined using a JOEL 1200 EX-2010 high resolution transmission electron microscope (HR-TEM) operating at 200 kV. This was pre-equipped with SAED analyzer Cu grid which was coated by SCCQDs and then TEM was done. Mechanistic studies were done through SCIEX QIDA-TOF Mass Spectrophotometer (Model: X500R; m/z : 100-1000 Da; 0.151 min) and ^1H (500 MHz) NMR spectrophotometer (Model-ECZ-500R) in D_2O taking TMS as an internal standard. The CHN Analysis of SCCQDs was done using CHN Analyzer (Model-CE-440 Elemental Analyzer Exeter Analytical, Inc.). The Raman analysis was performed by LabRAM HR Evolution Horiba Raman spectrophotometer (Model: E200R). CHN analysis was performed by Elemental Analyzer Exeter Analytical (Model: CE-440).

S2. Absorption Spectra and Tauc Analysis

It was observed that 0.1 g of CM could expel 0.095 g of residue through carbonized residue in 10 mL of deionized water (on stirring for 30 min); thereby extracting 0.008 g of SCCQDs. The concentration of the prepared dilution was found to be 6.25 mg L⁻¹ as per following calculations:

Amount of residue obtained from 30 mg CM = 28.5 mg

Amount of SCCQDs transferred to aqueous medium = 1.5 mg

Concentration of 10 mL SCCQDs stock solution = 1.5 mg/10 mL = 0.15 mg mL⁻¹

Amount of SCCQDs in 0.125 mL of this stock solution = 0.15 mg mL⁻¹ x 0.125 mL = 0.01875 mg

Concentration attained when 0.125 mL SCCQDs stock solution is diluted to 3 mL = 0.01875/3 = 0.00625 mg mL⁻¹ = 0.00625 mg mL⁻¹ x 1000 mL = 6.25 mg L⁻¹

Absorption coefficient (ϵ) and optical density for the amorphous QDs are used to calculate optical band gap (E_g) by knowing the photonic energy ($h\nu$) as,

$$[(\alpha - \alpha_s)h\nu]^{1/n} = \beta(h\nu - E_g) \dots \dots \dots \mathbf{1}$$

which is called Tauc relation, where α_s is the minimum absorption coefficient of solvent, β is band tailing parameter, and n is power factor (equivalent to 1/2, 3/2, 2, or 3 for direct allowed, direct forbidden, indirect allowed and indirect forbidden transitions) respectively. Tauc plots *i.e.*, plot of $[(\alpha - \alpha_s)h\nu]^{1/n}$ vs. $h\nu$, for $n = 1/2$ and their extrapolation up to $[(\alpha - \alpha_s)h\nu]^{1/n} = 0$ is used to deduce E_g and β for these transitions. The degeneracy of the states can be calculated using Boltzmann distribution. Transition population and %Transition allowance is calculated as,

$$\text{Transition population} = \left(\frac{N_n}{N_0} \right) = (2l + 1) e^{\Delta E_g/k_B T} \quad l = 0(S), 1(P), 2(D) \dots \dots \dots \mathbf{2}$$

$$\% \text{Transition allowance} = \frac{\Delta E_g}{k_B T} \times 100 \dots \dots \dots \mathbf{3}$$

where l , E_g , k_B , T refers to level coefficient, semiconductor band gap obtained from Tauc plot, Boltzmann's constant, and absolute temperature, respectively.

Table S1: Absorption peaks observed in the Absorption spectra of SCCQDs with various excitonic parameters

No. of peaks	1st Peak	2nd Peak	3rd Peak
Absorbance wavelength; λ_{abs} (nm)	298.24	232.26	206.39
Absorbance; A	0.057	0.107	0.167
Transmittance; $T = 10^{2-A}/100$	0.877	0.782	0.667
Reflectance; $R = 1 - (A+T)$	0.066	0.111	0.157
Specific Absorption coefficient; $\epsilon_{\text{sp}} = A/cl(L \text{ gcm}^{-1})$	9.12	17.12	26.72
Absorption factor; $f = 1-10^{-\epsilon cl}$	0.123	0.218	0.319
Transition Band Gap; $\Delta E(\text{eV})$	2.46 (E_g)	4.88	5.36
Singly degenerate population; $(N_n/N_o)_{g=1} = e^{E/k_B T}$	5.424	4.17	1.239
Area of transition peak; $(N_n/N_o)_{g'}$	3.507	3.00683	-
Degeneracy; $g' = (N_n/N_o)_{g'} \times e^{-E/k_B T}$	0.978 (1)	2.778 (3)	-
Degeneracy term; $l = (f-1)/2$	0 (S)	1 (P)	-
Transition Allowance; $TA = 100 \times \Delta E_{\text{eh}}/k_B T(\%)$	56.097	90.240	209.750

The direct allowed transition band gap is calculated for all three excitonic transitions through Tauc's plot. Thereafter, the transition population fraction (N_n/N_o) can be calculated using Boltzmann relation, assuming that the transition energy levels are singly degenerate $[(N_n/N_o)_{g=1}]$. However, single degeneracy is beyond reality, so to estimate the transition population is estimated through peak area analysis $[(N_n/N_o)_{g'}]$. The area of all the three peaks is estimated through OriginPro 6.1. As the third peak is incomplete (i.e., λ_{ex} : 206.39 nm) its area calculation is avoided. Thereafter, degeneracy and degeneracy term are calculated through this peak area. Transition allowance is also calculated.

S3. Fluorescence Maxima Estimation

The fluorescence maxima *i.e.*, the wavelength for maximum fluorescence, is deduced by recording the fluorescence spectra for a particular concentration of analyte over different excitation wavelengths in the region of absorption maxima. For carbohydrate derived CQDs the excitation range varies from 330 to 390 nm. In our case, as the absorption maxima was observed at 298 nm, the excitation wavelengths should range between 290-390 nm.

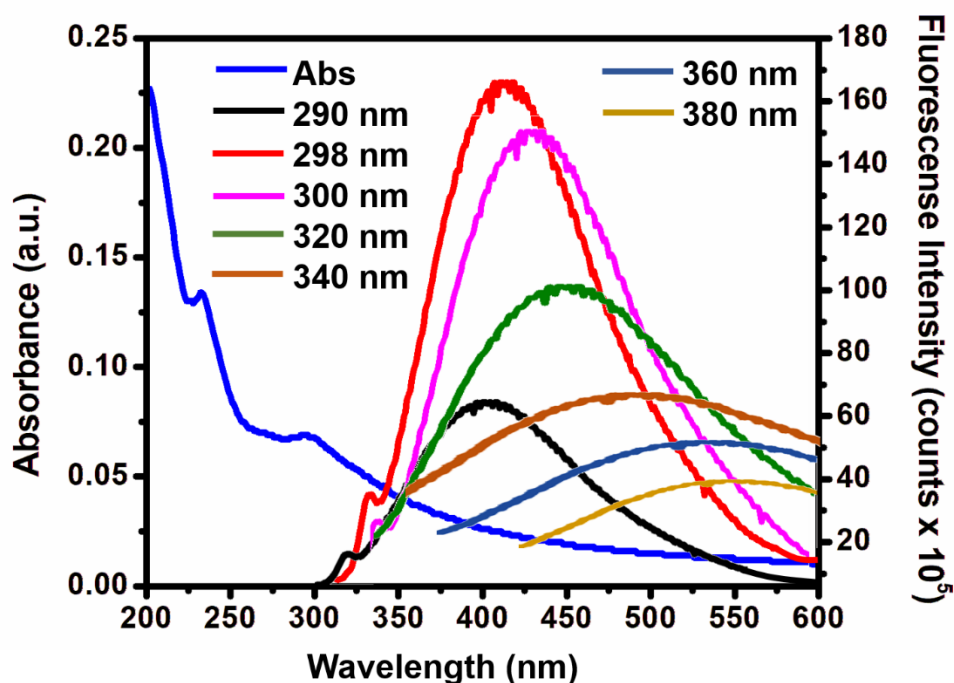


Figure S1: Emission maxima estimation for SCCQDs 6.25 mgL⁻¹ solution (290-380 nm)

Table S2: Excitation, Start and emission maxima wavelengths for the 6.25 mgL⁻¹ SCCQDs solution

Excitation wavelength (nm)	Emission maxima (nm)	Fluores. Intensity (counts x 10 ⁵)
290	398	64
298	408	167
300	425 (Maxima)	158 (Maxima)
320	451	103
340	422	63
360	512	45
380	526	38

S4. Quantum Yield Estimation

The quantum yield (QY) performed against solutions (2.083-10.417 mg L⁻¹) against similar concentrations of aqueous solution (λ_{em} : 464 nm; ϵ : 17.75 L g⁻¹cm⁻¹). It's the ratio of the number of photons emitted by a material to the number of photons absorbed by it during excitation.

$$\phi_m = \phi_R \times \left(\frac{\int F_M d\lambda}{\int F_R d\lambda} \right) \times \left(\frac{1-10^{-\epsilon_R c l}}{1-10^{-\epsilon_M c l}} \right) \times \left(\frac{\mu_M}{\mu_R} \right)^2 \dots\dots\dots 4$$

where $\phi_{m\ or\ R}$, $\int F_{M\ or\ R} d\lambda$, $\epsilon_{M\ or\ R}$, $\mu_{M\ or\ R}$, C , F and l refers to QY, area of emission peak, absorption coefficient, density, concentration spectrally integrated photon flux at the detector (the area under the emission spectrum corrected for blank emission and the wavelength dependence of the instrument's spectral responsivity), and path length of the absorption cuvette for analyte (M) and standard (R). In its superscript, ϵ equals the molar decadic absorption coefficient, c the chromophore concentration, l the optical path length.

Table S3: Calculation of %QY of diluted SCCQDs samples *w.r.t.* diluted (Quinine SO₄) QS solutions, (c , $A_{em.}$, and f represents concentration, Area of emission spectra & $1-10^{-\epsilon c l}$)

c (mg L⁻¹)	$\lambda_{em.}$ (CQDs) (nm)	A_{em} (CQD) (x 10⁻⁷)	A_{em} (QS dil) (x 10⁻⁷)	f_{CQDs}	f_{QS}	ϕ_{CQD}	% ϕ_{CQD} (%ϕ_{QS}: 54)
2.083	407	0.6509	10.1117	0.0427	0.082	0.068	12.30
4.167	406	0.9024	12.3343	0.0837	0.1565	0.074	13.67
6.250	407	2.1834	14.3635	0.1229	0.2254	0.150	27.88
8.330	410	1.5994	17.0012	0.1605	0.2889	0.091	16.93
10.417	413	1.4032	18.1345	0.1965	0.347	0.099	18.51
CQDs:	$\lambda_{em.}$: 408 nm(Avg.); ϵ_{sp} : 9.12 L gcm ⁻¹ ; $\lambda_{ex.}$: 298.2 nm						
QS:	$\lambda_{em.}$: 464 nm(Avg.); ϵ_{sp} : 17.75 L gcm ⁻¹ ; $\lambda_{ex.}$: 346.6 nm						

S5. Powder X-ray Diffraction

Crystallite size have been conventionally calculated through powder-XRD spectra using the famous Debye-Scherrer Equation, in terms of full width at half maxima (FWHM i.e., β_{eli} in radians), in relation with particle size (D, in nm), *i.e.*,

$$\beta_{\text{eli}} = \frac{K\lambda}{D \cos \theta} \dots \dots \dots 5$$

Where K, θ , refers to proportionality constant (~ 0.9) and scattering angle (in radians). For quantum mechanical systems, with crystallite size $D < 10$ nm, the obtained FWHM (β_{total}) includes error due to strain. In order to calculate strain-free D, Williamson and Hall formulated a relation that relates strain originated FWHM to scattering angle θ and the strain (ϵ) as:

$$\beta_{\text{strain}} = c\epsilon \tan \theta \dots \dots \dots 6$$

where, c is a proportionality constant equal to 4.0. Total broadening is referred to as:

$$\beta_{\text{total}} = \beta_{\text{eli}} + \beta_{\text{strain}} = \frac{K\lambda}{D \cos \theta} + c\epsilon \tan \theta \dots \dots \dots 7$$

Multiplying $\cos \theta$ both sides, we get Williamson-Hall Equation:

$$\beta_{\text{total}} \cos \theta = \frac{K\lambda}{D} + c\epsilon \sin \theta \dots \dots \dots 8$$

Which is used to develop a linear fit plot between $\beta_{\text{total}} \cos \theta$ and $c \sin \theta$ with ϵ and KD/λ as slope and intercept, respectively. The slope of this equation provides the strain on the particle that can further be used to calculate elasticity, bulk and rigidity parameters through knowing mass of the NP, and its elastic compliances. The applicability of Williamson Hall approach is checked through the regression coefficient and value of strain obtained from its plot. The application of DS approach for CM and WH approach for SCCQDs is done on the basis of their crystallite size and effective strain, as a small crystallite size (< 1 nm) and strain ($< 10^{-4}$) reduces the WH equation to DS equation. However, at larger crystallite sizes (> 1 nm) and strain ($< 10^{-4}$) the electronic bombardment on QD-surface is not negligible, thus validating the WH approach. The negligible strain of the order $\epsilon \approx 10^{-4}$, would reduce second half of WH equation to 4×10^{-6} negligibly effecting the 1st half of equation of the order, $K\lambda/D \approx 10^{-2}$. Under such circumstances, $\epsilon \approx 0$, is considered and WH equation reduces to DS equation,

$$\lim_{\epsilon \rightarrow 0} \beta = \lim_{\epsilon \rightarrow 0} \left(\frac{K\lambda}{D \cos \theta} + 4 \epsilon \tan \theta \right) \approx \frac{K\lambda}{D \cos \theta} \dots \dots \dots 9$$

Table S4: PXRD characteristics of SCCQDs

PXRD parameters	SCCQDs
DS particle size (nm)	-
WH particle size (nm)	0.863
Electronic strain	3.33×10^{-3}
RMS strain	2.66×10^{-3}
Correlation coefficient	2.67
WH linearity	0.8541
Phase maxima	NGE
Phase nature	Amorphous

S6. XPS Spectroscopy

Pellets of the SCCQDs were prepared and vacuum dried before XPS analysis. Deconvolution was done using XPSPEAK41 software.

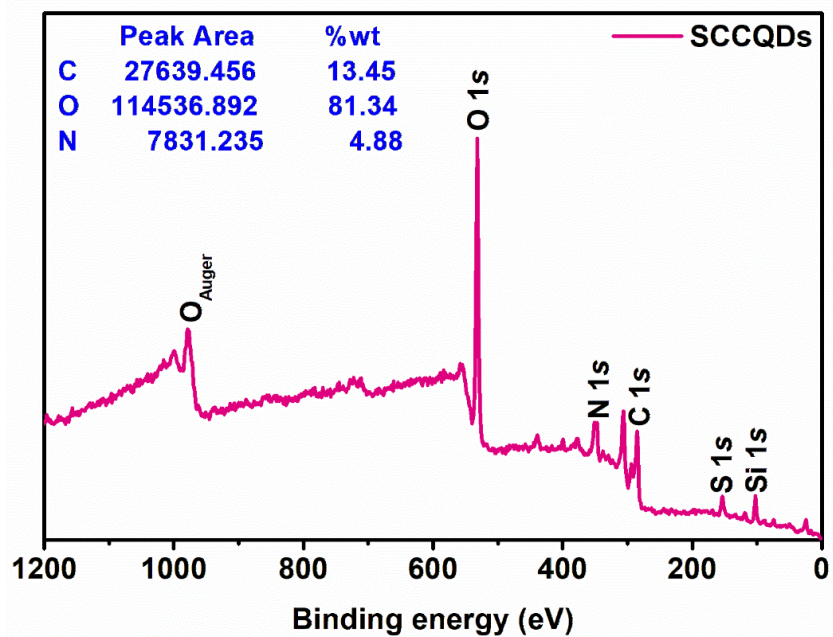


Figure S2: XPS spectrum of SCCQDs

S7. FTIR Spectroscopy

Dried KBr pellets of the following samples were prepared in order to analyze their FTIR spectra.

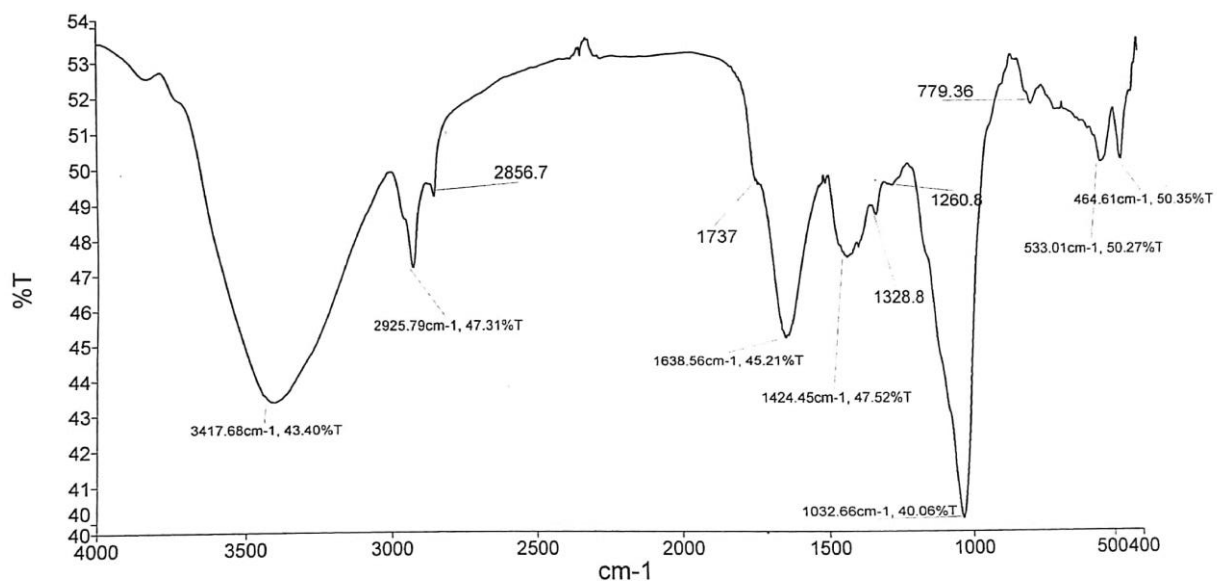


Figure S3: FTIR spectrum of sugarcane bagasse powder

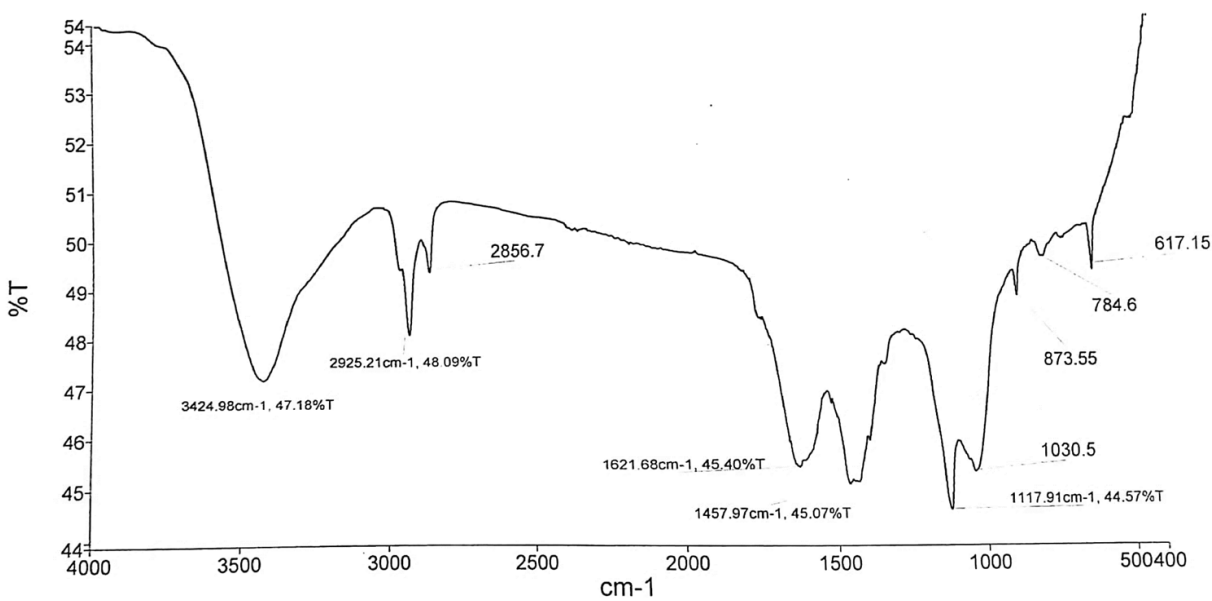


Figure S4: FTIR spectrum of collected SCCQDs

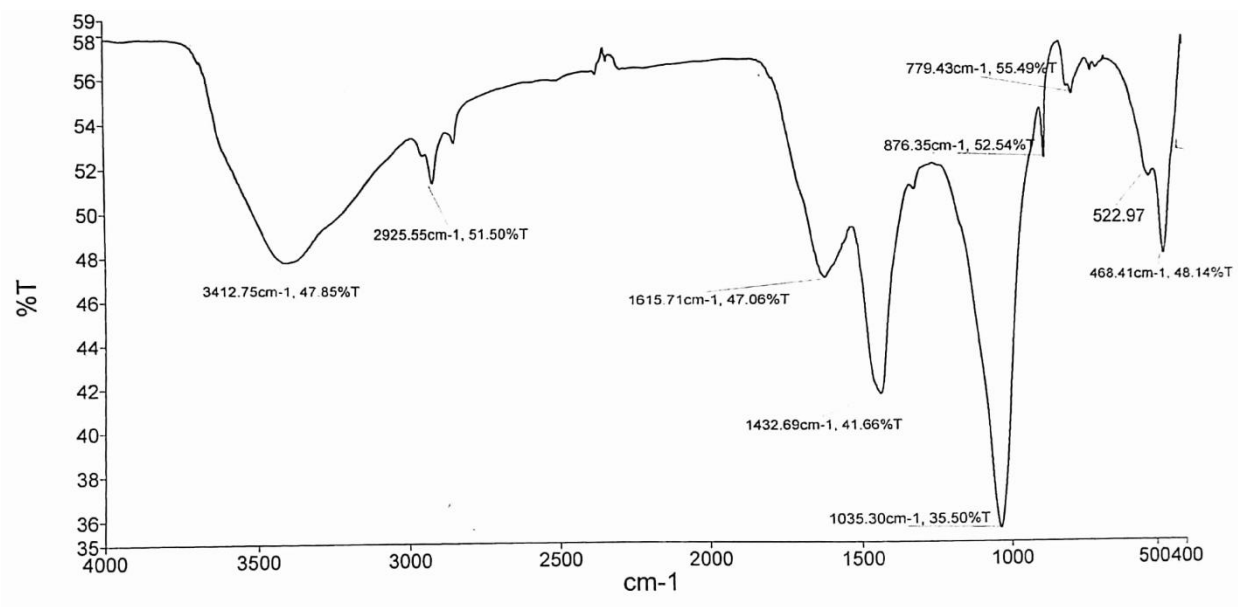


Figure S5: FTIR spectrum of the water insoluble residue obtained after collection of SCCQDs

Table S5: IR spectral data of different samples (ν : stretching and δ : bending modes)

Peak Assignment	Sugarcane bagasse powder (cm^{-1})	Extracted SCCQDs (cm^{-1})	Extraction residue (cm^{-1})
$\nu_{sym}(-OH)$	3417	3424	3412
$\nu_{sym}(-CH)$	2925	2925	2925
$\nu_{sym}(-CH)$	2856	2856	2856
$\nu_{sym}(C=O)$	1737	-	-
$\nu_{sym}(CO_2^-, cis C=C)$	-	1621	1615
$\nu_{sym}(-CH)_{inplane}$	-	-	-
$\delta_{sym}(OH); COOH$	1424	1457	1432
$\nu_{sym}(cyclicC-O)$	1328	-	-
$\nu_{asym}(C=C)$	1260	-	-
$\nu_{sym}(C-O)$	-	1117	-
$\nu_{asym}(C-O-C)$	1032	1030	1035
$\nu_{asym}(C=C) str.$	-	873	876
$\delta_{sym}(1,2disub-CH)$	779	784	779
Inorganic entrap	-	617	-
	533	-	522
	464	-	468

S8. Dynamic Light Scattering Analysis

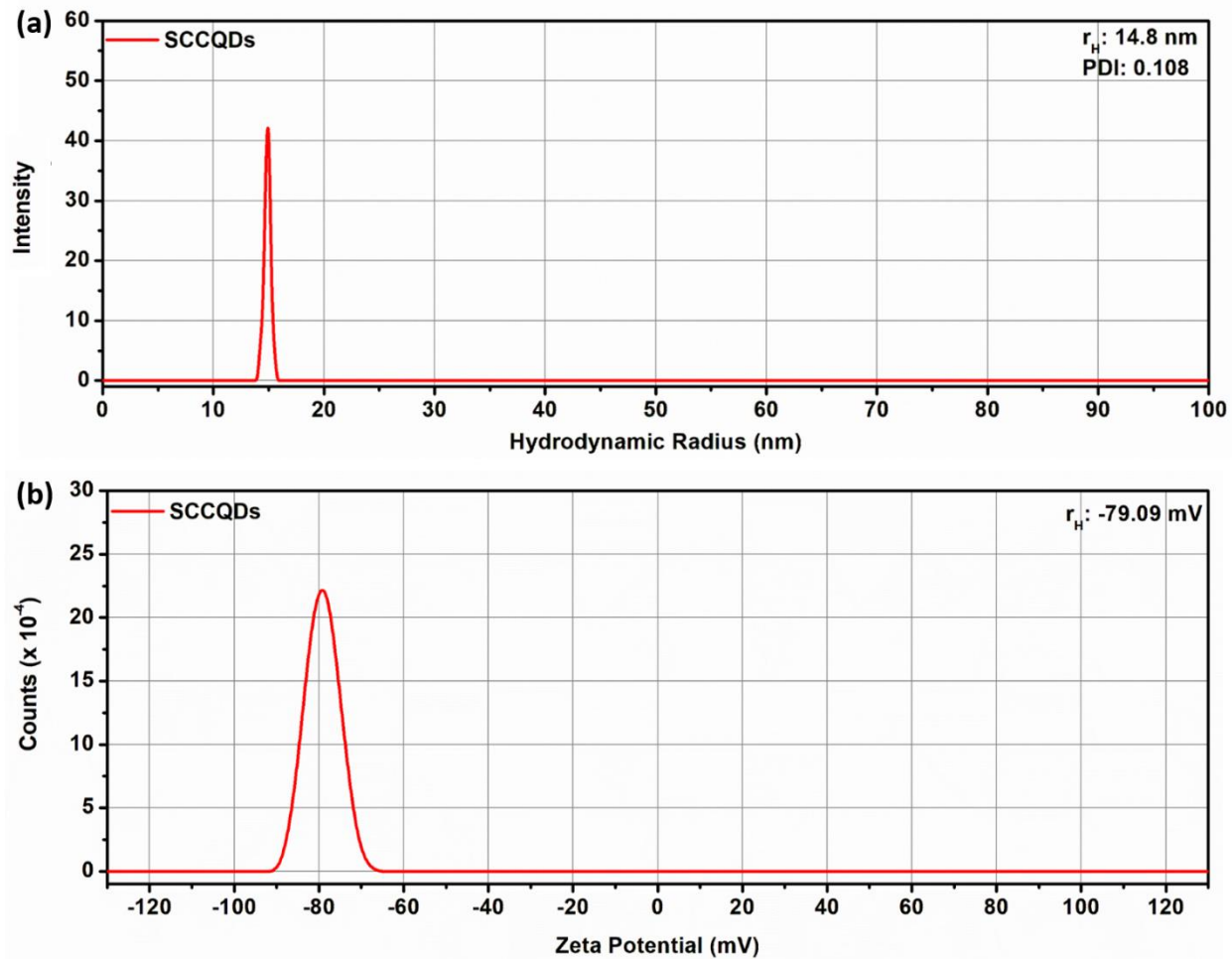


Figure S6: Dynamic Light Scattering pattern of SCCQDs; (a) Hydrodynamic radius; (b) Zeta Potential

S9. Brus Kayanuma Calculations

As per Wannier-Mott Hydrogen atom model the e/h pair mimics the hydrogen atomic system and its eigen value in terms of effective mass ($\mu = m_e m_h / (m_e + m_h) = x m'_e$) and orbital overlap approximation is given through the extended Brus Kayanuma (BK) equation *i.e.*,

$$(E_g - E_b - 0.25R_f)D^2 + \left(\frac{1.8e^2}{4\pi\epsilon_0\epsilon_r}\right)D - \frac{\hbar^2}{8xm'_e} = 0 \dots\dots\dots 10$$

where, E_g , E_b , R_f , e , ϵ_0 , ϵ_r , \hbar , m'_e and D refers to semiconductor bandgap (eV), bulk band gap (eV), Rydberg spatial function, electronic charge (1.602×10^{-19} C), permittivity of free space ($8.854 \times 10^{-12} \text{ m}^{-3}\text{kg}^{-1}\text{s}^4\text{A}^2$), dielectric constant of the medium, reduced Plank's constant ($6.58 \times 10^{-16} \text{ m}^2 \text{ kg s}^{-1}$) and electron rest mass (9.109×10^{-31} kg) and quantum system size ($\sim 10^{-9}$ m; which should be less than the material's Bohr's excitonic radii (R_{es}) calculated as $0.053\epsilon_r/x$), respectively. For conventional QDs Rydberg spatial function ($0.25R_f \rightarrow 0$) is negligible and dielectric constant is large, thereby giving rise to reduced BK equation (rBK), *i.e.*,

$$\frac{1}{D^2x} = \frac{8m'_e}{\hbar^2} (E_g - E_b) \dots\dots\dots 11$$

Where, $8m'_e/\hbar^2$ is called the RBK coefficient (rBKC = 10.59 nm^{-2}). The knowledge of reduced mass coefficient is necessary (x) which is calculating through Stokes shift relation *i.e.*,

$$x = \frac{\hbar^2\pi^2}{D^2m'_e} \times \left(\frac{c_{em}/c_{ex}}{\left(\frac{\hbar c}{\lambda_{em}} - \frac{\hbar c}{\lambda_{ex}}\right)}\right) \dots\dots\dots 12$$

where, c_{em} , c_{ex} , h and c refers to concentration for absorbance and emission spectra (for SCCQDs $\lambda_{ex} = 298 \text{ nm}$, $\lambda_{em} = 408 \text{ nm}$, $c_{ex} = c_{em} = 6.25 \times 10^{-3} \text{ g L}^{-1}$), Plank's constant ($6.626 \times 10^{-34} \text{ m}^2 \text{ kg s}^{-1}$), velocity of light ($2.99 \times 10^8 \text{ m/s}$) respectively. The reduced mass coefficient and bulk band gap (E_b) was found to be $0.069 m'_e$ and 1.01 eV , respectively. Thereafter, the dielectric constant of SCCQDs was calculated through solvation corrected BK equation (scBK) *i.e.*,

$$\frac{1}{D^2x} = \left[\frac{8m'_e}{\hbar^2} - \frac{4\pi\epsilon_0}{1.8e^2} \left(\frac{\epsilon_r}{Dx}\right)\right] (E_g - E_b) \dots\dots\dots 13$$

For water dispersible SCCQDs (with $1/D^2x = 0.78 \text{ nm}^{-2}$, $E_g = 2.46 \text{ eV}$, $E_b = 1.08 \text{ eV}$) ϵ_r was found to be equal to 1.099. Overall, 51% quantum confinement is attained in its synthesis.

S10. VMD Simulation of SCCQDs

The CQDs can be understood as a composition of multilayer circumcoronene graphene layers (CC-GLs) with a definite interlayer spacing. A model of CQDs with particle size 2.0 nm has been represented in Figure S6(a). The size of each CC-GL size symmetrically increases in size from the bottom-most (L_E) to the middle CC-GL (L_{ML}) and then symmetrically decreases in size up to the top-most CC-GL (L'_E). For such an arrangement, it becomes crucial for a CQD model to be composed of odd number of CC-GLs. Similarly, the edge-length of each CC-GL layer; comfortably represented as number of benzene rings (BRs), symmetrically increases from bottom L_E to L_{ML}

and then symmetrically decreases up to L_E . For simulation of such structure, it's crucial to know the number of CC-GLs, interlayer spacing of CC-GLs, Edge-length of each of the CC-GL layers.

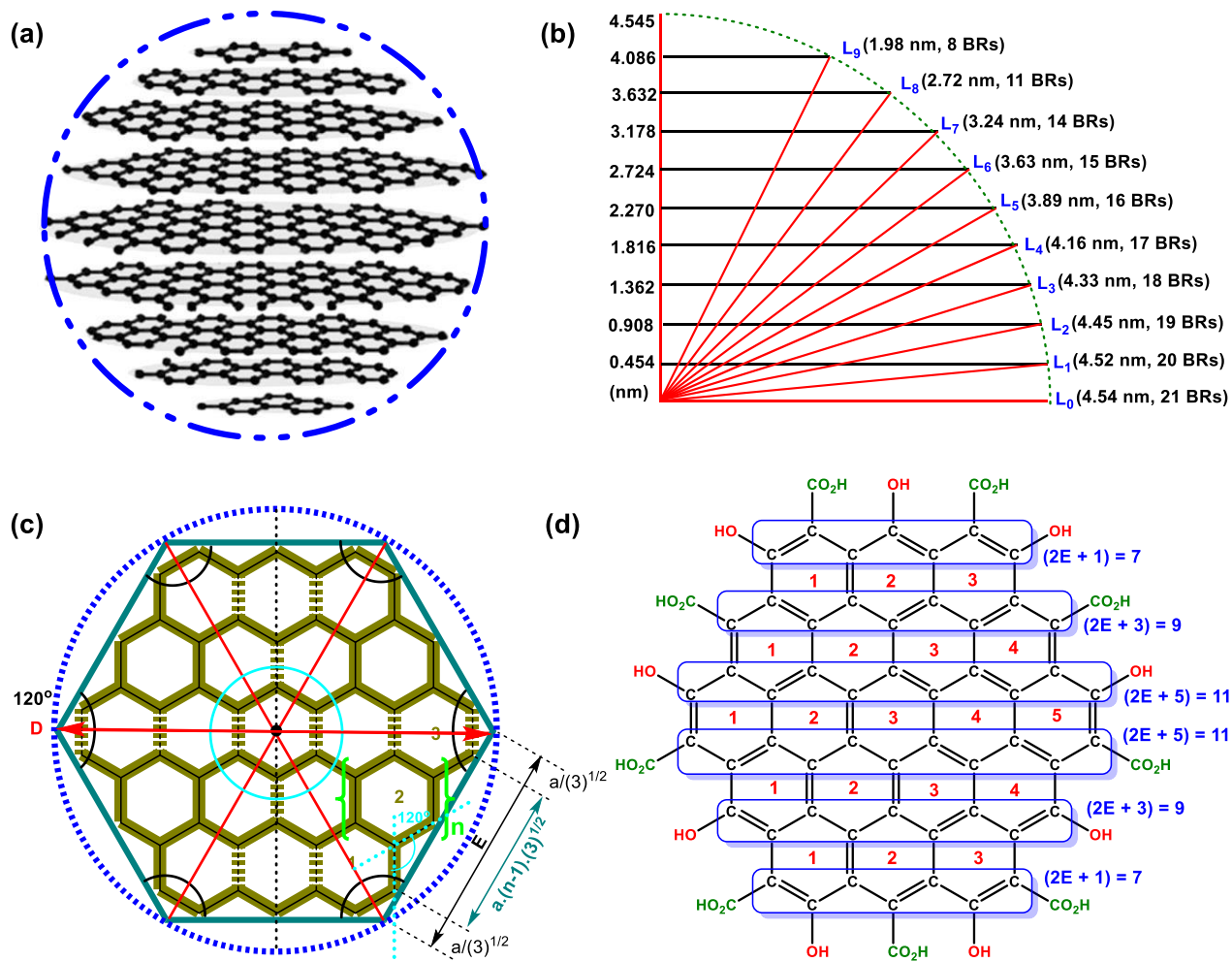


Figure S7: The illustration depicting the relation of SCCQDs particle size to number of benzene rings over CC-GL edges

At first, in order to estimate the number of CC-GLs in the SCCQDs, Kasper's relation for multilayer graphene systems were employed. Kasper's relation interrelates number of CC-GLs (n_L) of UMG type SCCQDs, to its particle size ($D = 9.09$ nm) as,

$$-\left(\frac{s}{2} + w\right) n_L^2 + (D - k) n_L - 2k = 0 \dots \dots \dots 14$$

Where, s , w and k refer to graphene parameters (0.1775, 0.1 and 0.16). The quadratic equation gives $n_L = 19.5$ and -16.2 . The negative number value of CC-GLs is absurd it is rejected. The value of 19.5 needs to be rounded off as fractional value of CC-GLs is again practically absurd. This value could either be rounded off to 20 or 19 and even number of CC-GL is not applicable for this

system, SCCQDs is considered to be formed of total 19 CC-GLs. With this, the interlayer spacing (δ) of SCCQDs was calculated to be 0.45 nm, by dividing its particle size by 19. Thereafter employing this data, the layer radius (B_n) for each of the layer (n) is trigonometrically calculated through,

$$B_n = \sqrt{\frac{D^2}{4} - (\delta n)^2} \dots\dots\dots 15$$

The edge length for each of the CC-GL can be trigonometrically calculated in terms of number of benzene rings (BRs) as per the spatial geometry of a typical CC-GL (Figure S6(b, c)),

$$D = \frac{4a}{\sqrt{3}} + (2E - 2)a\sqrt{3} \dots\dots\dots 16$$

where, D and a refers to the particle size of SCCQDs and bond length -C=C- of graphite (1.39 Å). Thereafter, the layer radius for the top-most CC-GL (B_9) and middle CC-GL (B_0) was found to be 4.54 nm and 1.98 nm, respectively. The edge-length (in terms of BRs) for middle CC-GL (L_0) and extreme CC-GLs (L_9) were found to be 21 and 8. It is also visible that till L_7 , there has been a sequential decrement in edge-length by one unit (of BR) up till L_9 . Thereafter L_7 , there has been an abrupt decrement in edge-length till L_9 . This abrupt decrement in the size of these layers tentatively suggests their high surface energy and poor stability. This suggests that these layers are weak surface sites from where surface weathering could initiate. Finally, the CQDs can be represented in terms of theoretical structure as, $[(n-1)/2 \text{ } |^{B_0} \text{ } | (n-1)/2]^d$; where, n : Number of CC-GLs; 0 : Middle Layer; B : Number of benzene rings in the CC-GL edge; D : Particle size of SCCQDs; d : Inter-layer distance. SCCQDs can be therefore represented as $[9 \text{ } |^{210_{9.09}} \text{ } | 9]^{0.454}$. Finally with this representation in hand, the SCCQDs were simulated using Open GUI VMD 9.3.1 software through Nanotube extension, developed by Otypeka *et al* (2018).

Thereafter, using the simulated structure the number of carbon, oxygen, hydrogen, carboxyl and hydroxide atoms/groups can be calculated. For this calculation a circumcoronene ring of edge-length 3 BRs. There are basically two types of carbons, the one in the ring (C_g) and the other as carboxyl functionality (C_{COOH}). The carbon atoms at the surface of the circumcoronene ring (C_s) consists of two types of carbons, the one that can be functionalized (C_{sf}) and the one that cant be functionalized (C_{suf}). The functionality of the carbon atoms that be functionalized has been done by alternative arrangement of carboxyl and hydroxyl groups, for the sake of simplicity. As represented in Figure S6(d), the number of C_g s (N_{C_g}) can be calculated as the double of the arithmetically progressing number of carbon atoms in the ring as a function of edge-length, represented as $(2E + 1)$, $(2E + 3)$, $(2E + 5)$, till the upper middle portion CC-GL. On summing the arithmetic progression of E number of terms, with first terms to be $(2E + 1)$ and term difference of 2, the $N_{C_g}^C$ can be calculated as

$$N_{C_g}^C = 2 \left[\frac{E}{2} (2[2E + 1] + 2[E - 1]) \right] = 6E^2 \dots\dots\dots 17$$

For further studies, circumcoronene rings with edge-lengths of 3, 4 and 5 BRs. For E = 3 BRs, number of surface carbon atoms (N^C_s), number of functionalized surface carbon atoms (N^C_{sf}), number of non-functionalized surface carbon atoms (N^C_{suf}) number of carboxyl (N_{COOH}), number of hydroxyl (N_{OH}) groups, number of oxygen atoms (N_o) and number of hydrogen atoms (N_H) was found to be 30, 18, 12, 9, 9, 27 and 18 respectively. For E = 4 BRs, $N^C_s = 42$, $N^C_{sf} = 24$, $N^C_{suf} = 18$, $N_{COOH} = 12$, $N_{OH} = 12$, $N_o = 36$, and $N_H = 24$. Similarly, E = 5 BRs, $N^C_s = 54$, $N^C_{sf} = 45$, $N^C_{suf} = 9$, $N_{COOH} = 15$, $N_{OH} = 15$, $N_o = 45$, and $N_H = 30$. Therefore, following formulations can be proposed,

$$N^C_g = 6(2E - 1) \dots\dots\dots 18$$

$$N^C_{sf} = 3E \dots\dots\dots 19$$

$$N^C_{suf} = 3(3E - 2) \dots\dots\dots 20$$

$$N_{COOH} = N_{OH} = 3E \dots\dots\dots 21$$

$$N_c = N^C_g + N^C_{COOH} = 6E^2 + 3E \dots\dots\dots 22$$

$$N_o = 9E \dots\dots\dots 23$$

$$N_H = 6E \dots\dots\dots 24$$

Thereafter, these values are calculated and represented in Table

Table S6: The Calculation following parameters for SCCQDs as per VMD simulation

Layer	E(BRs)	N^C_g	N^C_{COOH}	N^C_s	N^C_{sf}	N^C_{suf}	N_{COOH}	N_{OH}	N_c	N_o	N_H
L9	8	384	24	90	24	66	24	24	408	72	48
L8	11	726	33	126	33	93	33	33	759	99	66
L7	14	1176	42	162	42	120	42	42	1218	126	84
L6	15	1350	45	174	45	129	45	45	1395	135	90
L5	16	1536	48	186	48	138	48	48	1584	144	96
L4	17	1734	51	198	51	147	51	51	1785	153	102
L3	18	1944	54	210	54	156	54	54	1998	162	108
L2	19	2166	57	222	57	165	57	57	2223	171	114
L1	20	2400	60	234	60	174	60	60	2460	180	120
L0	21	2646	63	246	63	183	63	63	2709	189	126
L1'	20	2400	60	234	60	174	60	60	2460	180	120
L2'	19	2166	57	222	57	165	57	57	2223	171	114
L3'	18	1944	54	210	54	156	54	54	1998	162	108
L4'	17	1734	51	198	51	147	51	51	1785	153	102
L5'	16	1536	48	186	48	138	48	48	1584	144	96
L6'	15	1350	45	174	45	129	45	45	1395	135	90
L7'	14	1176	42	162	42	120	42	42	1218	126	84
L8'	11	726	33	126	33	93	33	33	759	99	66
L9'	8	384	24	90	24	66	24	24	408	72	48
Total		29478	891	3450	891	2559	891	891	30369	2673	1782

S11. CHN analysis of SCCQDs

Table S7: CHN analysis data for SCCQDs

SCCQDs (6.64 mg)					
Element (Retention time; min)	Number of Atoms	Simulated wt%	CHN analysis wt%	Number of atoms	Empirical Coefficient
Carbon (1.06)	30369	88.98549	88.922138	30390.6246	3
Hydrogen (5.67)	1782	0.50115	0.437801	1781.9989	
Nitrogen (0.76)	0	0.00000	0.190061	2.0003	
Oxygen	2673	10.51335	10.450000	2672.1995	

From the above data,

For Carbon, 88.922138% of 6.64 mg = 5.90443 mg

For Hydrogen, 0.437801% of 6.64 mg = 0.02907 mg

For Nitrogen 0.190061% of 6.64 mg = 0.01262 mg (nearly negligible; impurity)

For Oxygen 10.450000% of 6.64 mg = 0.69388 mg

From the above data,

$$\begin{aligned} \text{Number of Carbon atoms} &= 5.90443 \times 10^{-3} / 1.999 \times 10^{-23} \text{ (Mass of 1 Carbon atom) g} \\ &= 296705.13 \times 10^{15} \end{aligned}$$

$$\begin{aligned} \text{Number of Hydrogen atoms} &= 0.02907 \times 10^{-3} / 0.167 \times 10^{-23} \text{ (Mass of 1 Hydrogen atom) g} \\ &= 17410.14 \times 10^{15} \end{aligned}$$

$$\begin{aligned} \text{Number of Oxygen atoms} &= 0.69388 \times 10^{-3} / 2.657 \times 10^{-23} \text{ (Mass of 1 Oxygen atom) g} \\ &= 26115.21 \times 10^{15} \end{aligned}$$

$$\begin{aligned} \text{Number of Nitrogen atoms} &= 0.01262 \times 10^{-3} / 2.323 \times 10^{-23} \text{ (Mass of 1 Nitrogen atom) g} \\ &= 5439.68 \times 10^{15} \end{aligned}$$

$$\begin{aligned} \text{Molecular weight for 1 CQDs} &= (30369 \times 12) + (2673 \times 16) + (1782 \times 1) = \mathbf{408978 \text{ amu}} \\ &= 6.791 \times 10^{-19} \text{ g} \end{aligned}$$

$$\text{Number of SCCQDs in 6.64 mg of SCCQDs} = 6.64 \times 10^{-3} / 6.79 \times 10^{-19} = \mathbf{9.77 \times 10^{15} \text{ SCCQDs}}$$

S12. Calculation of E_{VB} and E_{CB} values

According to the previous literature, the potentials of valance edge potential (E_{VB}) and conduction edge potential (E_{CB}) of a semiconductor material could be calculated via the following empirical equations:

$$E_{VB} = \chi - E_e + \frac{1}{2} E_g \dots\dots\dots 25$$

$$E_{CB} = E_{VB} - E_g \dots\dots\dots 26$$

$$\chi = [x_C^{N_C/N_O} x_O^1] \exp\left(\frac{1}{N_C/N_O + 1}\right) \dots\dots\dots 27$$

$$x_C = \frac{1}{2} (IE_C + EA_C) \dots\dots\dots 28$$

$$x_O = \frac{1}{2} (IE_O + EA_O) \dots\dots\dots 29$$

where, IE_C , IE_O , EA_C , EA_O , χ , x_C , x_N , N_C , N_O , E_e refers to ionization energy of carbon (11.26 eV) and oxygen (13.16 eV), electron affinity of carbon (1.26 eV) and oxygen (1.46 eV), electronegativity of SCCQDs, electronegativity of carbon (6.26) and oxygen (7.31), calculated number of carbons (30369) and oxygen (2673), and free electrons on the hydrogen scale (4.5 eV), respectively. Electronegativity of SCCQDs was found to be 6.32 and this led to the $E_{VB} = 3.06$ eV and $E_{CB} = 1.56$ eV.

S13. Sunlight mediated Photodegradation of MB dye

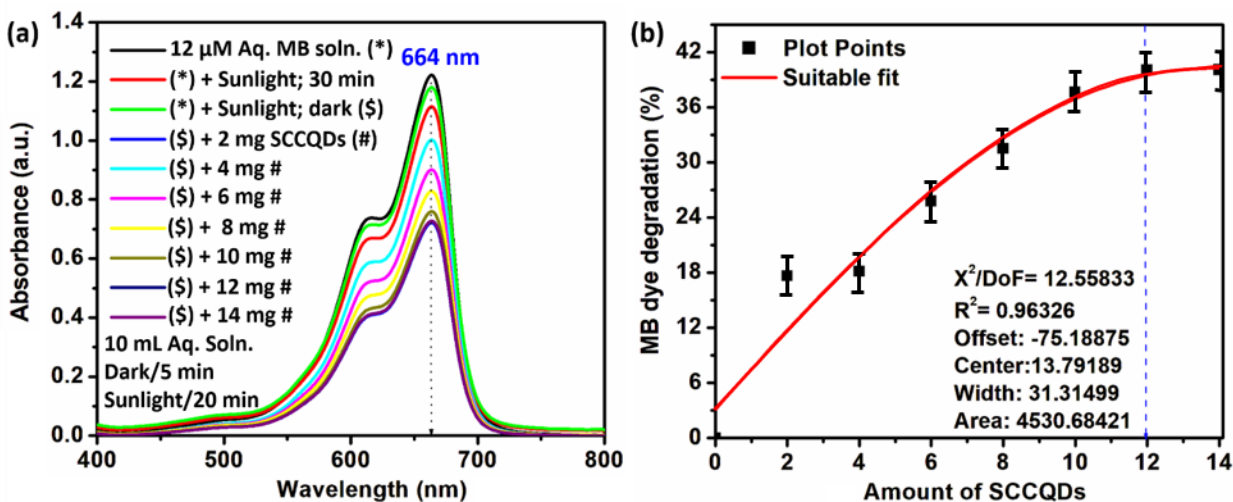


Figure S8: Estimation of photoactive amount of SCCQDs for sunlight mediated degradation of MB dye; (a) UV-Visible spectra; (b) Plot of %dye degradation vs. photocatalyst amount (mg)

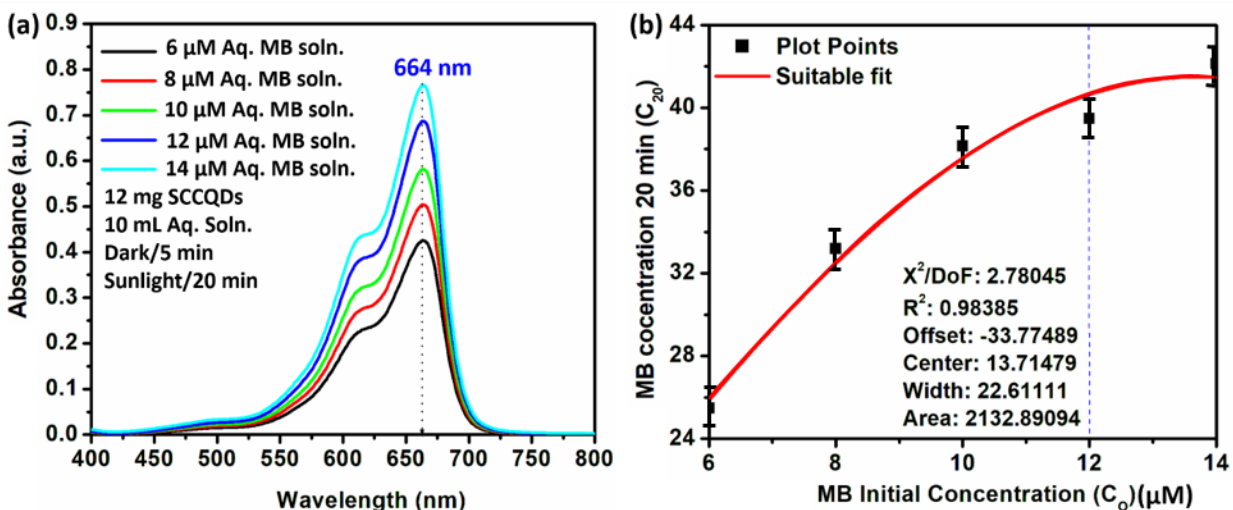


Figure S9: Estimation of maximum amount of MB that 12 mg of SCCQDs can degrade in sunlight; (a) UV-Visible spectra; (b) Plot of %dye degradation vs. initial MB concentration (μM)

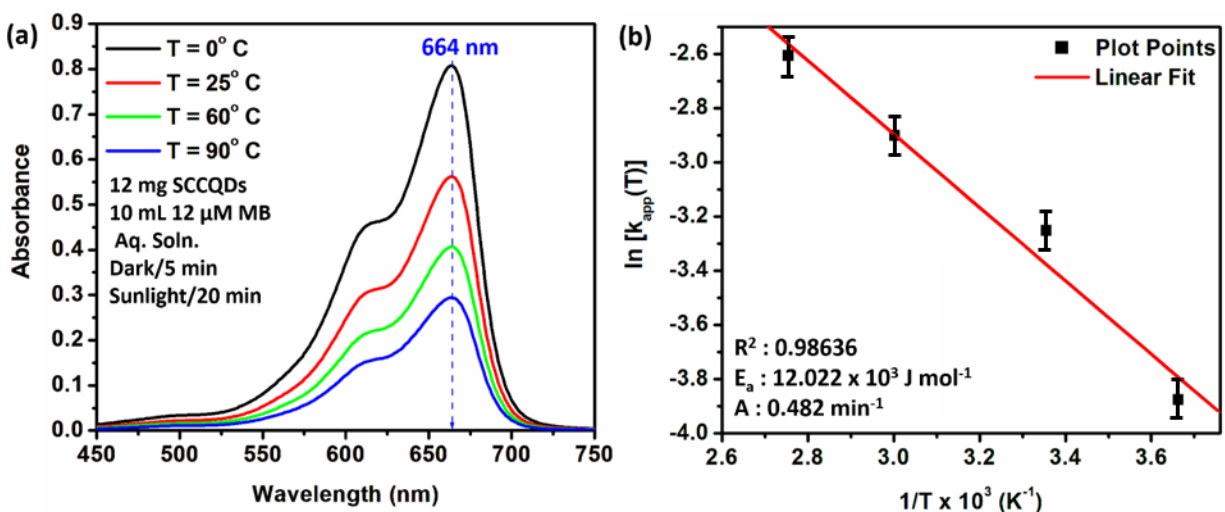


Figure S10: Optimized sunlight mediated MB dye degradation in presence of SCCQDs over various temperatures; (a) absorption spectra; (b) Plot of $\ln[k_{\text{app}}]$ vs. $1/T$ (K^{-1})

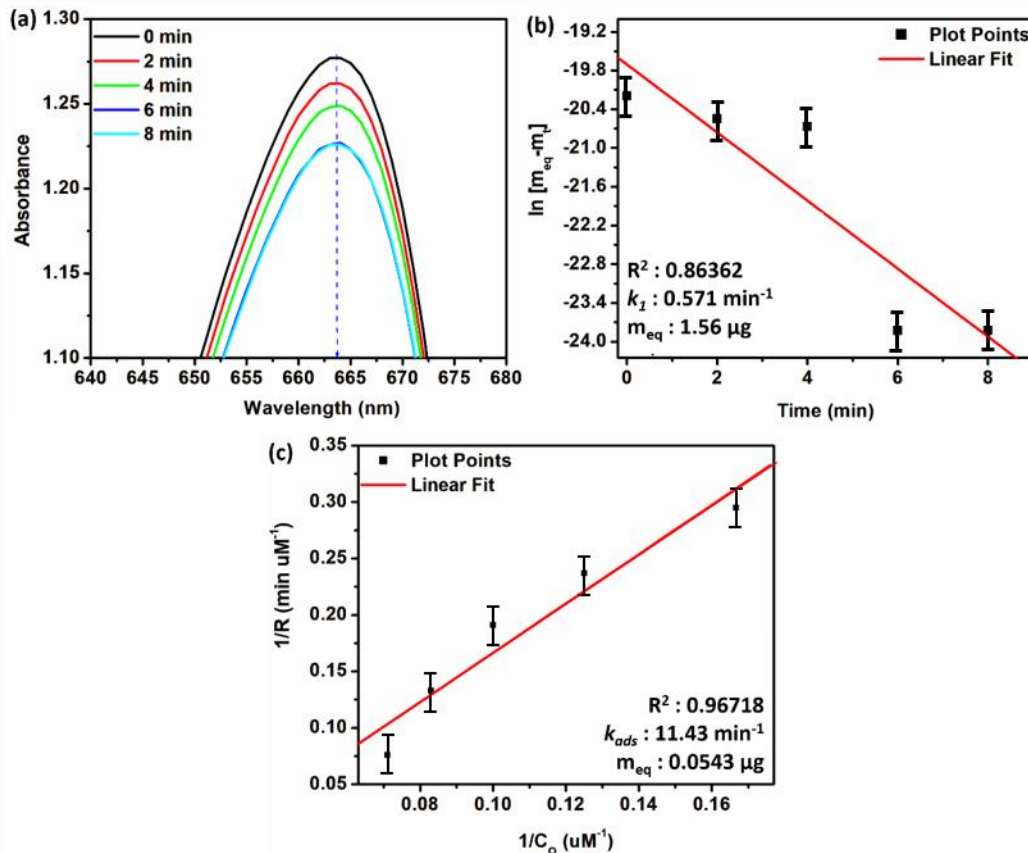


Figure S11: Adsorption analysis MB dye degradation in presence of SCCQDs in dark (a) UV-Visible spectra; (b) Plot of $\ln [m_{eq}-m_t]$ vs. t (min) to calculate adsorption rate constant; (c) Plot of $1/R$ (rate) vs. $1/C_o$ (initial concentration of MB) to calculate adsorption parameters.

Calculation of kinetics of the reaction wrt 1st order:

$\ln[A_t] = \ln[A_o] - k_{app}t$ and $t_{1/2} = 0.693/k_{app}$ **30**

Where A_t and A_o is the absorbance of MB at time $t = 0$ and $t = t$ minute; during dye degradation reaction.

Plot of $\ln [A_t]$ vs. t gives a linear plot for which Slope = k_{app} and intercept = $\ln [A_o]$

Calculation of thermodynamic parameters of MB degradation:

Arrhenius equation is given as,

$\ln k_{app} = \ln A - \frac{E_a}{RT}$**31**

Where, k_{app} , E_a , A , R , T , refers to rate of dye degradation at a given temperature, activation energy, Arrhenius constant, Gas constant and given temperature, respectively. The plot of $\ln k_{app}$ vs. $1/T$ gives a linear plot whose slope = E_a/RT and intercept = $\ln A$ respectively. Now at room temperature ($T = 298$ K),

$\Delta H^\ddagger = E_a - RT$**32**

$$\Delta S^\ddagger = R \ln k_{app} + \left(\frac{\Delta H^\ddagger}{T}\right) - R \ln \left(\frac{k_B}{h}\right) \dots\dots\dots 33$$

$$\Delta G^\ddagger = \Delta H^\ddagger - T\Delta S^\ddagger \dots\dots\dots 34$$

$$K^\ddagger = e^{-\Delta G^\ddagger/RT} \dots\dots\dots 35$$

Where, k_{app} , E_a , A , R , T , ΔH^\ddagger , ΔS^\ddagger , ΔG^\ddagger , k_B , h , K_Q refers to rate of dye degradation, activation energy, Arrhenius constant, Gas constant, temperature, enthalpy of activation, activation entropy, free energy of activation, Boltzmann constant, Plank's constant and equilibrium constant, respectively. The plot of $\ln k_{app}$ vs. $1/T$ gives a linear plot whose slope = E_a/RT and intercept = $\ln A$ respectively.

Calculation of Adsorption thermodynamics/kinetics:

As per Langmuir Hinshelwood mechanism,

$$\frac{1}{R} = \frac{1}{k_{ads}} + \frac{1}{k_{ads}K_{ads}} \left(\frac{1}{C_0}\right) \dots\dots\dots 36$$

$$\Delta G^\circ = -RT \ln[K_{ads}] \dots\dots\dots 37$$

where, R , k_{ads} , K_{ads} refer to C_0 rate of dye degradation, rate constant for monolayer adsorption of MB over SCCQDs, equilibrium constant for dye adsorption, and initial dye concentration respectively. Plot of $1/R$ and $1/C_0$ gives a linear plot with slope = $1/k_{ads}K_Q$ and intercept = $1/k_{ads}$.

As per Largargren 1st order adsorption kinetics,

$$\ln[m_{eq} - m_t] = \ln[m_{eq}] - k_1 t \dots\dots\dots 38$$

where, m_{eq} , m_t and k_1 amount of MB dye in solution phase at equilibrium and at time t and 1st order adsorption rate constant, respectively. The plot of $\ln [m_{eq} - m_t]$ vs. t gives a linear plot with slope = k_1 and intercept = $\ln [m_{eq}]$.

S14. Analysis of SCCQDs-R5

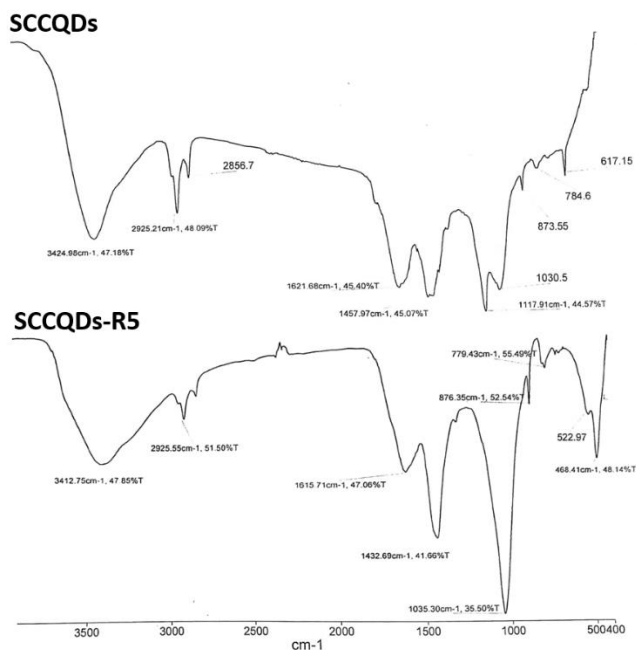


Figure S12: Comparative FTIR spectra of fresh SCCQDs and SCCQDs-R5 obtained after recycling from MB dye degradation

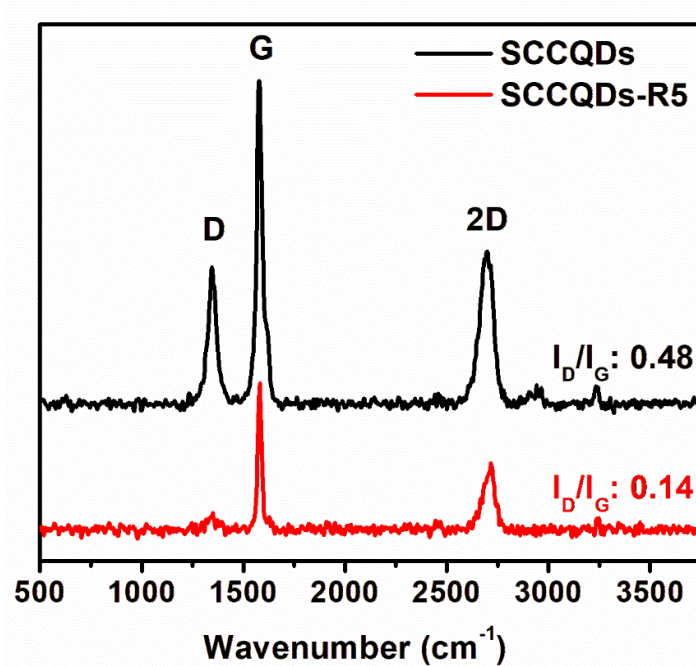


Figure S13: Comparative Raman spectra (Excitation: 532 nm) for fresh SCCQDs and SCCQDs-R5 obtained after recycle from MB dye degradation reaction

S15. Mechanistic study of MB dye degradation

The mechanistic studies of the SCCQDs-catalyzed room-temperature mediated MB dye degradation was studied by placing two sets of the optimized reaction in D₂O. At time intervals t = 0, 12, 24 and 36 min, about 700.0 μL of reaction aliquots were taken out and syringe filtered. The 10.0 μL of these syringe filtered reaction aliquot is added with 900.0 μL of methanol and the obtained mixture was submitted for HRMS analysis. Another 600.0 μL of the syringe filtered reaction mixture was submitted for ¹H NMR analysis. Thereafter, the HRMS spectra was directly obtained from the spectrometer machine. The obtained ¹H NMR spectra was analyzed and the spectral prediction of degradation intermediates were simulated and stacked on MestReNova 14.1.2.25024 NMR analyzer.

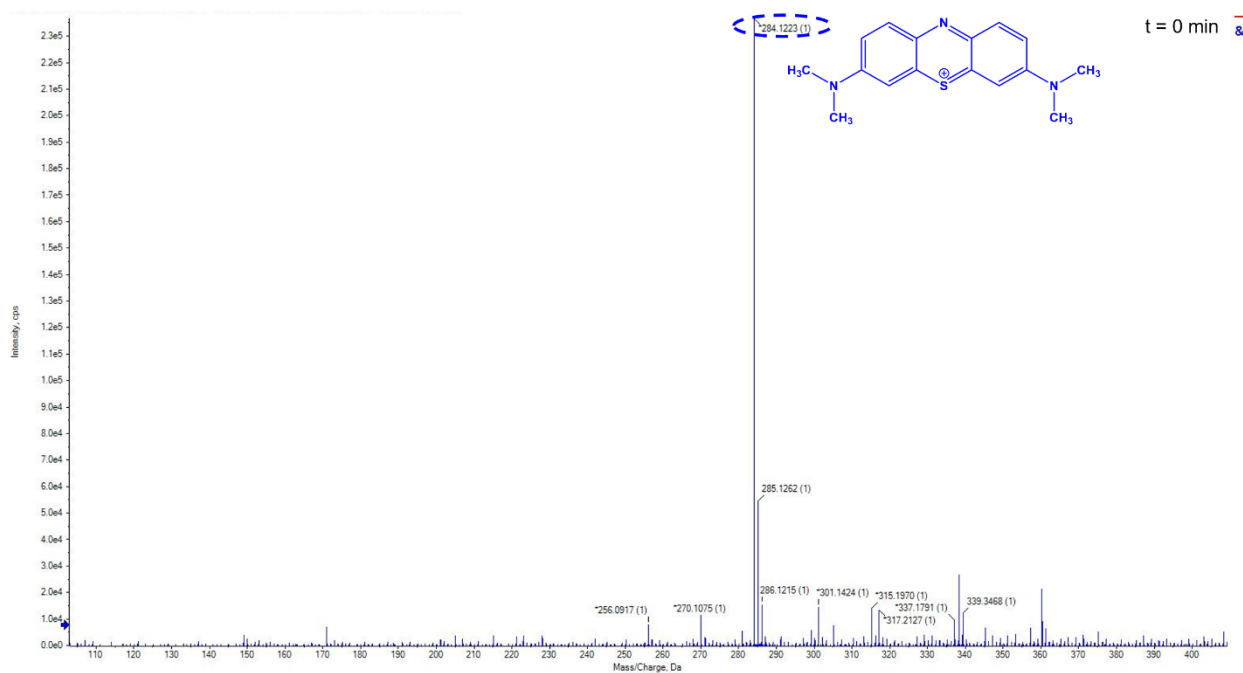


Figure S14: HRMS spectra of reaction aliquot at t = 0 min

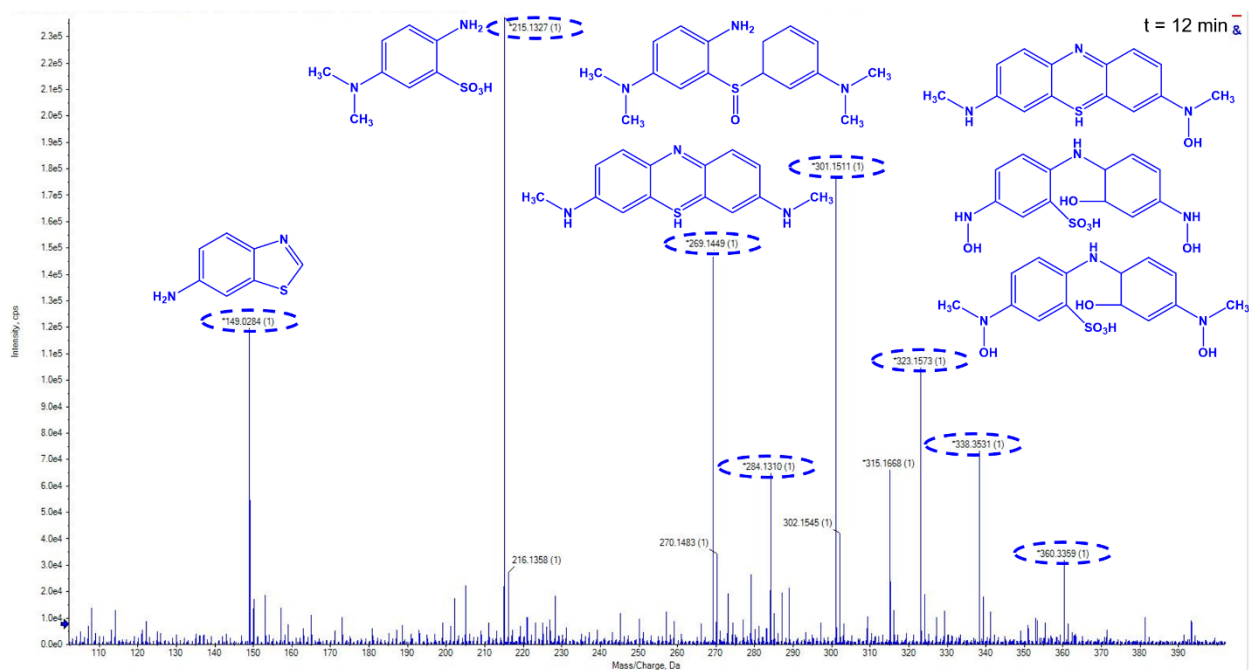


Figure S15: HRMS spectra of reaction aliquot at t = 12 min

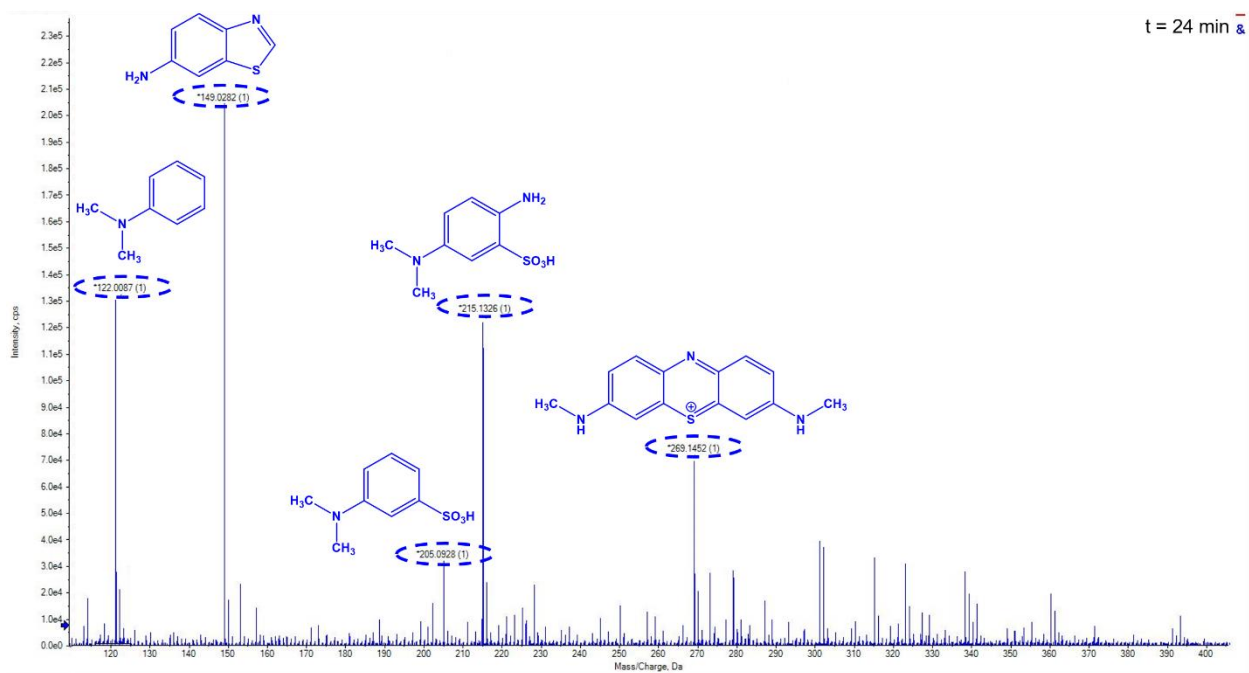


Figure S16: HRMS spectra of reaction aliquot at t = 24 min

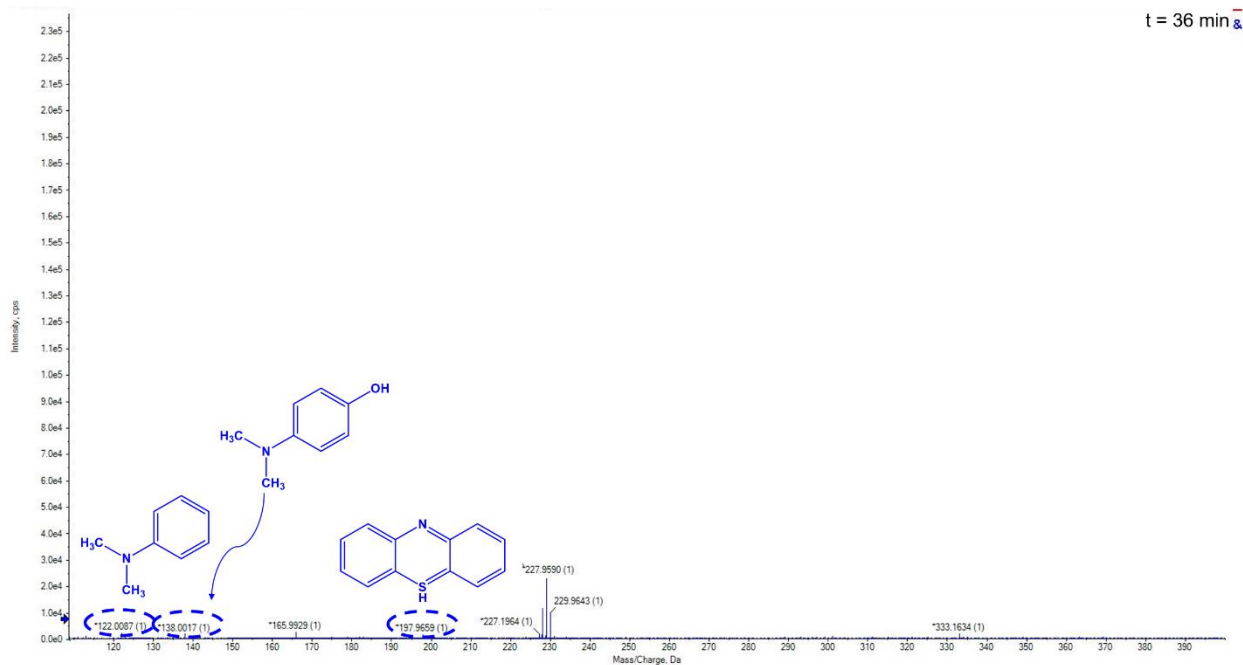


Figure S17: ^1H NMR spectra of reaction aliquot at t = 36 min

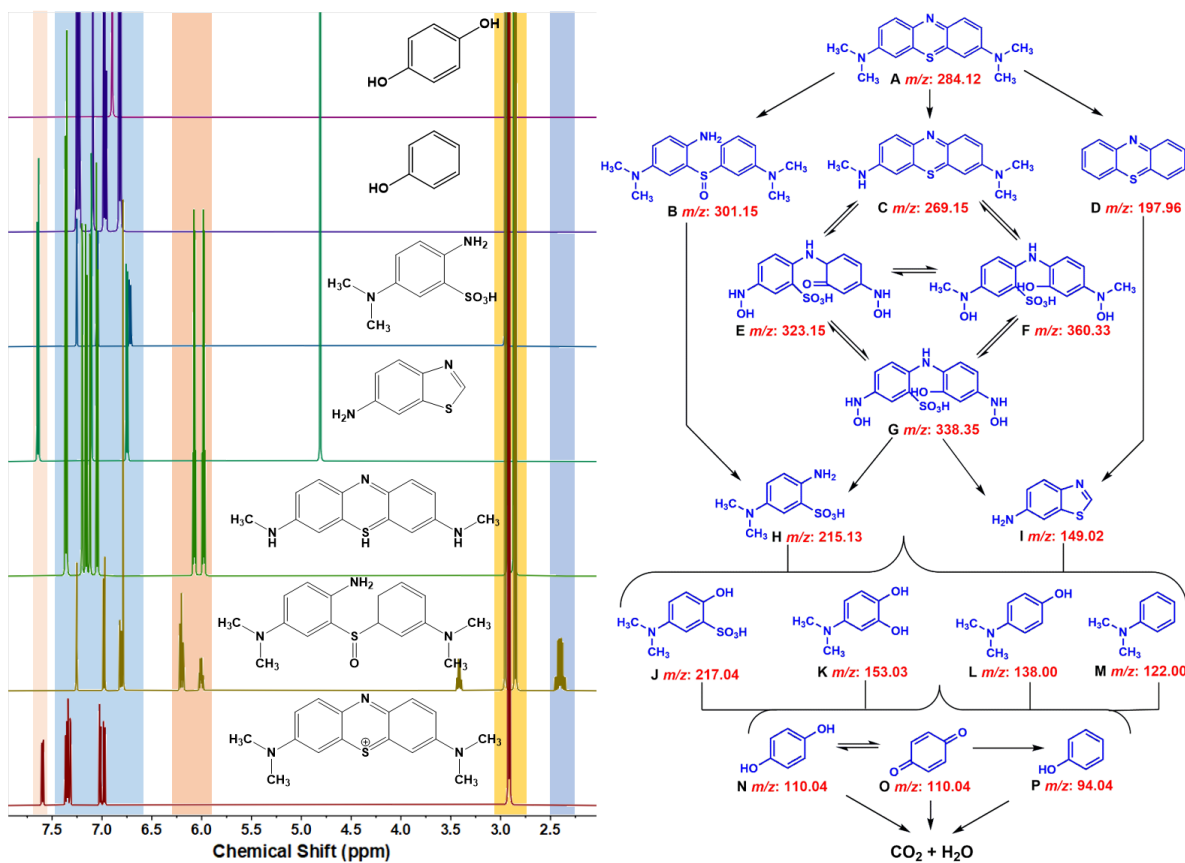


Figure S18: Predicted ^1H NMR spectra stacked over one another and comparison with experimental spectra in main manuscript

S16. Previous reports synthesis and application of Sugarcane bagasse derived CQDs

Table S8: Comparison of previous reports on sugarcane bagasse derived CQDs and their applications with the SCCQDs prepared in this study

Research Group	CQDs (size (nm); shape; QY; E _g ; I _b /I _G)	Synthesis	$\lambda_{ex}/\lambda_{em}$ (nm)	Application	Remarks	Ref.
Gupta <i>et al</i> (2024)	SCCQDs (9.09 nm; s; 2.46 eV; 0.48)	H(3 g/12.5 mL H ₂ O; 500 °C; 6 h)	298/408	MB dye degradation ([CQD]: 12 mg; [MB]: 10 mL 12 μ M; t: 3h; RT; sunlight; recycle: 4)	Metal-free CQDs for photocatalytic 100% degradation with mechanistic study	TW
Parveen <i>et al</i> (2024)	sc-CQDs (27 nm; s)	H(6 g/20 mL 1M NaOH; 200°C; 4 h)	353/450	Antioxidant DPPH activity (EC ₅₀ : 2.8); MB dye reduction ([MB]: 30 μ M / 3 mL; [NaBH ₄]: 100 mM/300 μ L; [sc-CQDs]: (10 mg/mL) 300 μ L; t: 12 min; RT	Borohydride mediated reduction of MB via sc-CQDs and antioxidant activity	1
Luo <i>et al</i> (2024)	CQDs/ZnO NRs (3.2 nm; s; 4.07 eV)	ZnO/ 2% CQDs [H(1 g SB/ 30 mL H ₂ O; 180°C; 12 h)]	222/525	Organic Photo-detection: NEP and D* increased by 2.95 times	Metal oxide defects enhanced on doping via CQDs	2
Arsad <i>et al</i> (2023)	CQDs	H(3 g SB/ 2 g CA/NH ₄ OH (pH: basic/ 25 mL H ₂ O; 160°C; 6 h)	282/332	Synthesis of CQDs using SB pulp, <i>O. sanctum</i> , <i>C. sinensis</i> plant extract	Focuses on synthesis of CQDs from biomass and bio-extracts	3
Saravaran <i>et al</i> (2023)	CD/Polyester composite	Polyester/7 %-CDs P(SB; 450°C; 50 min; Ball Milling: 40 min)	-	Electrical conductivity, thermal conductivity, and mechanical strength of polymer improved	Composite material was tested against ASTM composite standards	4
Alfi <i>et al</i> (2022)	NCDs/paper (<10 nm; s; 24.8%)	H(0.2 g CDA (SB/TBAA:DMS O::2:8; 30 min; 60 °C. Ac ₂ O; 3 h; 60 min)/20 mL H ₂ O; 240° C; 14 h)	260/350	SFQ of tetracycline in the range of 0.01-150 μ M; LOD: 0.01 μ M. Photo-chromic blue emission was quenched	Paper coated SB CQDs coated dipsticks for tetracycline SFQ for photostability of up to 15 cycles	5

Qiu <i>et al</i> (2022)	gCQDs (2.79 nm; s; 2.24%)	H(4 g/ 80 mL H ₂ O; 220°C; 10 h)	369/437	SFQ of Fe ⁺³ ion (LOD: 1.47 μM)	Ligno-cellulosic CQDs from cassava stem, sorghum, SB, rubber, poplar, chinese fir SFQ for Fe ⁺³ were compared.	6
Du <i>et al</i> (2022)	N-CQDs (3.33 nm; s; 0.53)	H(1 g SB/1 g urea/30 mL H ₂ O; 260°C; 10 h)	268/417	SFQ detection of Fe ⁺³ ion (80%; LT: 7.19 ns)	N-doping provides coordination sites for Fe ⁺³ , facilitating their sensing	7
Kasinathan <i>et al</i> (2022)	CQDs (2-8 nm; s; 14.12; 0.84%)	H(1 g SB/ 1 g CA/ NH ₄ OH/50 mL H ₂ O; 200 °C; 4 h)	242/360	SFQ of Hg ⁺² ion (LOD: 0.1 μM), bioimaging of MCF-7 cancer cells	This semi-green study incorporates CA for better Hg ⁺² sensing	8
Nugraha <i>et al</i> (2021)	N-CQDs/WO ₃ (QD: 5 nm; s), (WO ₃ /N-CQDs: 200-300 nm; nano-sheets; 1.49 eV)	WO ₃ / 1% N-CQDs [H(300 mg SBBC(MF; 600°C; 1 h)/0.5 M, 30 mL NaOH/EDA (2.5 % w/v; 190 °C; 24 h)	350/603	Aq. Phase MB dye degradation ([Cat]: 0.6 g/L; [MB]: 5 ppm/100 mL; LS: 80 W Phillips lamp; t: 4h; Rec: 3 cycles)	CQDs over metallic oxide matrix achieved degradation (> 3 h) via anthropogenic light source	9
Nugraha <i>et al</i> (2021)	NH ₂ -CQDs (4.19 nm (EDTA) or 9.70 nm (EDA); s; 21.2%)	H(300 mg SBBC (SB; 600°C; 1h)/EDA(2.5-10%) or EDTA (1-3%)/ 30 mL 0.5 M NaOH; 190°C; 24 h)	250/500	Synthesis of CQDs containing -NH ₂ groups for N-functionalization of CQDs	Synthesis was done using SBBC for better attainment of better quantum confinement	10
Pandiyan <i>et al</i> (2020)	CQDs (2.57 nm; s, 17.98%)	H(2 g SB/2 g CA/NH ₄ OH (pH: 7)/25 mL H ₂ O; 200 °C; 6 h),	332/420	Antibacterial activity [G+ (<i>B. cereus</i> , <i>S. aureus</i>), G- (<i>P. aeruginosa</i> , <i>V. cholerae</i> , <i>E. coli</i>)]	Employs antioxidant CA for CQD-synthesis and achieve bio-activity	11
Chai <i>et al</i> (2019)	GQDs (2.26 nm; s)	H(3 g SB/40 mL H ₂ O; 180°C; 4 h; 1.7 °C/min)	338/428	Optimizing sugars, GQDs and porous carbon synthesis from SB	Synthetic optimization study detailed	12

					through BET, BJH, HR-TEM analysis	
Chung <i>et al</i> (2019)	CD/HAP (142 nm length; 20 nm width; rod)	Ca(NO ₃) ₂ .4H ₂ O + (NH ₄) ₂ HPO ₄ + 50 mL 0.4 M HCl + 500 mL 0.7 M NaOH + CDs (H(0.25 g/30 mL 0.5 M NaOH; 190°C ;24 h)); 16 h	225/515	Fall in fluorescence with release of drug acetaminophen through Diffusion controlled Higuchi Mechanism	The incorporation of CDs into HAP greatly increases the surface area from 41.631 to 54.095m ² g ⁻¹ and 78.752 m ² g ⁻¹ , giving the nanomaterial a greater drug loading capacity.	13
Baweja <i>et al</i> (2019)	SB-CQDs (3-5 nm; s; 25.7%)	P(500 mg SBBC(SB; 60°C; 1h); 50 mL PhMe; stir; 24 h)	350/435	Synthesis of SB derived CQDs and comparison of their photoluminescent properties with graphene derived CQDs	Photoluminescent properties of CQDs were much better than graphene derived CQDs	14
Eslami <i>et al</i> (2018)	CQDs (4-9 nm; flaky; 0.87)	H(supernatant (1 g acid treated SB(5 g SB/30 mL 98% H ₂ SO ₄ ; RT; 24 h)/80 mL 0.5 M NaOH; Reflux; 5h)/30 mL 0.5 M NaOH; 180°C; 24 h)	-	Adsorption of Naphthalene from aqueous solution	Adsorption studied through various adsorption isotherms at various naphthalene concentrations over various pH	15
Huang <i>et al</i> (2017)	SCM-CQDs (1.9 nm; s)	H(5 g SM/10 mL H ₂ O; 250°C; 12 h)	320/390	SFQ of Fe ⁺³ (0-100 μM) and sunset yellow (0-60 μM); biocompatibility and bioimaging of MCF-7, RBCs and BSA	Molasses derived CQDs used for SFQ and bioimaging studies of cells	16
Thambiraj <i>et al</i> (2016)	SCB-CQDs (4.1 nm; s; 18.7%; 0.85)	2g SBBC(MF; 60°C; 2h)/200 mL PhMe; stir; 24 h)	283/327	CQDs synthesis using SCB was performed	QY, application of CQDs, hydrodynamic properties are yet to be measured	17

Sun <i>et al</i> (2014)	CDs (1.8 nm; s; 12.3%; 0.5)	H(1 g SB/ 1M 20 mL NaOH; 180°C; 3h)	275/390	Multichannel fluorescent probes for multicolor tracking agents in flow cytometer	Green method for bio-imaging of MCF-7 cells with no cytotoxicity	18
-------------------------	-----------------------------	-------------------------------------	---------	--	--	----

1. S. Parveen, N. Bukhari, N. Ramzan, S. Musaddiq, S. Mubarak, A. Kalsoom, W. A. Qureshi, *Sugar Tech*, 2024, **26**, 1, 33–44.
2. Z. Luo, C. Wu, M. Yan, X. Yu, X. Yu, Q. Qian, Y. Zhou, H. Zhang, Z. Li, G. Long, *Materials Chem. Phys.*, 2024, **316**, 129056.
3. S. Arsad, *NJESR*, 2023, **5**, 6, 1-10.
4. K. Saravanan, D. J. Balakrishnan, K. Bhaskar, S. Madhu, *Biomass Conver. Biorefinery*, 2023, **2023**.
5. A. A. Alfi, N. A. Alamrani, O. A. Azher, R. M. Snari, H. M. Abumelha, Z. A. Al-Ahmed, N. M. El-Metwaly, *J. Mater. Res. Tech.*, 2022, **19**, 4697 -4707.
6. Y. Qiu, D. Li, Y. Li, X. Ma, J. Li, *Cellulose*, 2022, **29**, 367–378.
7. F. Du, M. Zhang, X. Li, J. Li, X. Jiang, Z. Li, Y. Hua, G. Shao, J. Jin, Q. Shao, M. Zhou and A. Gong, *Nanotechnology*, 2014, **25**, 31, 315702.
8. K. Kasinathan, S. Samayanan, K. Marimuthu, J.H. Yim, *Appl. Surf. Sci.*, 2022, **601**, 154266.
9. M. W. Nugraha, N. H. Z. Abidin, Supandi, N. S. Sambudi, *Chemosphere*, 2021, **277**, 130300.
10. M. W. Nugraha, N. S. Sambudi, L. D. Kasmiarno, N. A. Kamal, *ASEAN J. Chem. Eng.*, 2021, **21**, 1, 62-72.
11. S. Pandiyan, L. Arumugam, S. P. Srirengan, R. Pitchan, P. Sevugan, K. Kannan, G. Pitchan, T. A. Hegde and V. Gandhirajan, *ACS Omega*, 2020, **5**, 30363–30372.
12. X. Chai, H. Hea, H. Fana, X. Kang, X. Song, *Bioresource Tech.*, 2019, 282, 142-147.
13. H. K. Chung, V. Wongso, N. S. Sambudi, Isnaeni, *J. Sol-Gel Sci. Tech.*, 2020, **93**, 214–223.
14. H. Baweja and K. Jeet, *Mater. Res. Express*, 2019, **6**, 8, 850.
15. A. Eslami, S. M. Borghei, A. Rashidi and A. Takdastan, *Separ. Sci. Tech.*, 2018, **53**,16, 2536-2549.
16. G. Huang, X. Chen, C. Wang, H. Zheng, Z. Huang, D. Chen and H. Xie, *RSC Adv.*, 2017, **7**, 47840.
17. S. Thambiraj, D. R. Shankarana, *Appl. Surf. Sci.*, 2016, 390, 435-443.
18. S. Sun, S. Guo, Q. Qin, Y. Liao, M. Li, F. Du, *Chemosensors* 2022, **10**, 453.